Applied Energy 183 (2016) 380–389

Contents lists available at ScienceDirect

Applied Energy

journal homepage: www.elsevier.com/locate/apenergy

Recording frequency optimization for massive battery data storage in battery management systems

Yuejiu Zheng [a,b], Minggao Ouyang [b,*], Xiangjun Li [c,**], Languang Lu [b], Jianqiu Li [b], Long Zhou [a], Zhendong Zhang [a]

[a] College of Mechanical Engineering, University of Shanghai for Science and Technology, Shanghai 200093, PR China
[b] State Key Laboratory of Automotive Safety and Energy, Tsinghua University, Beijing 100084, PR China
[c] State Key Laboratory of Control and Operation of Renewable Energy and Storage Systems, Electrical Engineering and New Material Department, China Electric Power Research Institute, Beijing 100192, PR China

HIGHLIGHTS

- Flexible recording frequency approach is applied for low frequency signals.
- The most dynamic period is analyzed with DWT and FFT for high frequency signals.
- The mean absolute derivation method verifies the most dynamic period by DWT.
- Recording at 1 Hz is not enough for voltage and current during the dynamic period.
- The optimal recording frequency will not influence the SOC estimation accuracy.

ARTICLE INFO

Article history:
Received 12 April 2016
Received in revised form 4 August 2016
Accepted 25 August 2016

Keywords:
Battery management system
Data storage
Massive data
Recording frequency
Wavelet analysis

ABSTRACT

Massive data storage is an advanced function in a fully functional battery management system (BMS). Reducing the recording signal length undoubtedly saves the precious memory space for BMS. And it also reduces the network and computation loads. However, it leads to a side effect that the trend of signal distortion is enhanced. The optimal recording frequency in practice should be as low as possible on the condition that little signal distortion happens. This paper presents a novel method which uses a multi-frequency recording technology that cooperates two approaches according to the signal dynamics. A flexible recording frequency method is applied for stationary signals which only records signals when their values are changed. While for dynamic signals, the most dynamic period is found using discrete wavelet transformation (DWT) and further analyzed by fast Fourier transformation (FFT). By comparing two recording signal indicators for four different recording frequencies, we conclude that recording at 1 Hz is not qualified for the cell voltage and current during the dynamic period in our system due to the high dynamic performance of the vehicle. In the demonstrated vehicle, only by increasing the recording frequency to at least 2 Hz, can the accuracy of the recorded cell voltage achieve the level the same as the measurement accuracy in engineering. And we also verify that when the recording frequency is reduced to the optimal frequency compared to the high frequency recorded original signals, the accuracy of the SOC estimation is not influenced.

1. Introduction

With the rapid progress in lithium ion battery chemistry, large scale electric energy storage becomes possible nowadays. Large battery packs such as battery energy storage stations or electric vehicles (EVs) consist numerous battery cells [1,2]. However, cells always have inevitable variations which may come from manufacturing process or the operation environment [2–5]. A battery management system (BMS) is therefore required to manage and monitor all cells as well as the overall states of the battery pack. A fully functional BMS should fulfil the following requirements:

(1) Sensing and monitoring: all kinds of BMSs at least monitor the total current, the total voltage, voltages and temperatures of

* Corresponding author.
** Corresponding author.
E-mail addresses: yuejiu.zheng@gmail.com (Y. Zheng), ouymg@tsinghua.edu.cn (M. Ouyang), li_xiangjun@126.com (X. Li).

http://dx.doi.org/10.1016/j.apenergy.2016.08.140
0306-2619/

individual cells, as well as temperatures of the specified nodes in air [6]; (2) Power management: good power management will not only improve the life of battery packs or reducing the charging cost [7,8] but also precisely detect battery cell parameters by specific methods [9,10]; (3) State estimation: state of charge (SOC), state of health (SOH) and state of function (SOF) are calculated and are extensively investigated in literature [6,11,12]; (4) Thermal management: good thermal management guarantees preference temperature to make battery packs work well and temperature uniformity between cells is a more critical issue for better thermal management [13]; (5) Communication: as the modular topology is commonly applied in the BMSs, CAN (Controller area network) bus, the most typical communication link in the automotive environments, is commonly used in BMSs [14]. Daisy chained network is also a current focus in engineering for the BMS network. The future networks could be Flexray [15], and wireless commutation also draws much attention; (6) Cell balancing: BMS needs to equalize the cells in order to maximize the battery's capacity and life [16,17]; (7) Fault detection: battery system faults can be generally categorized into two types: system related faults and battery related faults which are intensively studied [18,19].

Massive data storage is an extended and advanced function in BMS. A fully functional BMS may record history data including the signals of total voltage, total current, cell voltages, cell temperatures and states such as pack and cell SOCs as well as cell balancing currents and so on. These data are recorded in a block of the BMS master controller which is specialized for data recording or a data logger controller linked to the master controller through the network. A secure digital memory card (SD card) or other memory storage devices are commonly used to store the data in the data logger, and it can be read on a PC for further research or for the maintenance of the battery pack [18]. With the progress in wireless communication, data transferred and saved into the server through wireless networks, e.g. 3G or 4G, is the newly developed technology for massive data storage. Though not all types of the BMSs have the function of massive data storage, it is very important for the BMS to record battery data during the operation in order to thoroughly analyze the battery performance off line:

(1) As one of the most important part in big data digging for energy storage systems, the recorded data provide real working conditions of the battery packs. Data in EVs contain the information of the vehicle power demands and the driving habits as well as the charging habits of the EV users. Micro grid power demands can be revealed by analyzing data in battery energy storage stations.
(2) Precise working conditions of battery packs from the stored data support the further development of EVs and other energy storage systems with improved data-driven algorithms [12,20,21], and as well as academic study of battery pack ageing [22].
(3) When battery system failures occur in some instances, the stored data can be used to investigate the origins of the faults and help to reduce similar failures in the future. For example, if we would have more comprehensive data during the battery fire accident in Boeing 787 (ANA 787 on January 16, 2013), causes of the fire might have been directly revealed instead of inferring conclusions from the post-mortem battery pack [23].

A data logger needs to record hundreds to thousands of signals according to the size of the battery packs. For example, in a small pack with 96 cells in series, at least 400 signals are typically required to be recorded including the total voltage and current, cell voltages, cell temperatures, balancing currents, cell SOCs and some control state signals et al. [18]. For large packs, e.g. a battery energy station with 20 battery strings in parallel and each string with 240 cells in series [1], the order of magnitude of the recording signals will be a ten thousand.

Data from a demonstrated EV in our experiments show 434 signals were recorded with 1 Hz recording frequency, and 2 signals ware were recorded with 4 Hz (the total current and voltage). The recording time was 26 days and recording a signal at a time takes an average of 8 bytes. To calculate the memory space the data takes, we use the following the equation.

$$M = nTfm \tag{1}$$

where M is the total memory space the data take, n is the number of signals, T is the total recording time, f is the recording frequency and m is the memory space it takes to record a signal at a time. Data of 26 days occupied 7.4 Giga Bytes (GB), i.e. completely full memory space of an 8 GB Secure Digital Memory Card (SD card). It was not a coincidence that the SD card was full, because the earlier data were covered by the incoming data.

Because the number of signals is predetermined by the design of the battery pack system, it is an effective way to reduce the recording frequency in order to increase the total recording time for the limited memory space in BMS. On the one hand, reducing the recording frequency will increase the capability of the recording time. As a result, some data logger set the recording period to 1 min or even longer [1]. But on the other hand, dynamic working condition in EVs requires fast recording of the current and voltage so as to ensure that no distortion happens to the recording signals. Typically, the recording frequency is set to 1 Hz [24] or even 10 Hz for this purpose.

In conclusion, reducing the recording frequency increases the total recording time but also increases the tendency of signal distortion according to the Shannon's sampling theorem. Conversely, increasing the recording frequency decreases the tendency of signal distortion but also decreases the total recording time. Therefore, the optimal recording frequency in practice should be as low as possible on the condition that no signal distortion happens. The benefits of reducing recording signal length without signal distortion are to save the memory space for memory stick devices and to reduce the network load. Besides, the additional benefits are:

(1) For off-line data processing, less data means faster and easier data processing.
(2) More importantly, the battery data are required to be stored in the memory space of the BMS microcontrollers for on-line calculation with some slightly more sophisticated functions. For example, cell voltage interpolating, charging curve fitting or on-line data-driven battery parameter estimation [12,25], they all need to recall the saved battery data from the Flash to the RAM (Random-Access Memory) and then calculated by the core of the microcontrollers. Obviously, the precious resources of RAM (currently less than 8 MB in most applications) as well as the computation capability limit the size of the recorded data. By optimizing the recording frequency, RAM as well as the computation capability will be greatly saved and more efficiently used.
(3) With the increasing popular wireless networks (e.g. 3G or 4G), cloud storage and computing are becoming feasible for vehicle application [26]. As the wireless flow is expensive at present, reducing recording signal length will undoubtedly save the cost of the cloud storage system.

This paper presents a novel method which uses a multi-frequency recording technology according to the signal dynamics. For stationary signals, a flexible recording frequency method is applied which only records signals when their values are changed. For dynamic signals, firstly, the most dynamic period is revealed

Table 1
Features of the multi-frequency recording method.

	Multi-frequency recording	
	Flexible recording frequency	Recording frequency optimization
Signal dynamic property	Stationary/low frequency	Dynamic/high frequency
Typical application	Temperature, SOC, current and voltages during stationary charging	Current and voltages during dynamic charging/discharging
Method	Recording signals and the corresponding time when their values are changed. The recording frequency is not predetermined, and is variant	Optimal recording frequency is predetermined by signal FFT analysis to ensure that the most dynamic period of the signal will not be distorted

using discrete wavelet transformation (DWT). Subsequently, its frequency is analyzed by fast Fourier transformation (FFT). And finally, the recording frequency is optimized according to the Shannon's sampling theorem.

2. Multi-frequency recording method

Because signals in BMS have different dynamics, e.g. temperature is commonly stationary while the current can be very dynamic, we present the multi-frequency recording method for signals with different dynamics. The principle of the method is simple: low frequency recording for low frequency signals and high frequency recording for high frequency signals. A flexible recording frequency technology for stationary signals is in low frequency domain. Recording frequency optimization for dynamic signals is in high frequency domain.

Therefore, before we use the multi-frequency recording method, dynamic properties of the signals in BMS should be discussed. The most important signals in BMS are the total current and voltage, and cell voltages are also essential in order to analyze cell variations and faults. Because the total and cell voltages directly correlate with the current as a natural property of the battery system, voltages and current are in the same frequency domain. It means that if we have optimized the recording frequency for the current, the same recording frequency can be used for the voltages. In most vehicle and energy storage applications, current varies in different working conditions. Battery working conditions can be categorized into three states: dynamic charging/discharging, stationary charging and standing by [18]. Current is in the high frequency domain during dynamic charging/discharging, and enters the low frequency domain during stationary charging and standing by.

Because temperature change of 1 °C has very little influence on the battery behavior, the temperature resolution of 1 °C is considered to be sufficient for BMS. High specific heat capacity, relatively low heat generation and good heat dissipation condition make relatively slow temperature change in BMS. As a result, temperature can always be considered as a stationary signal. Similarly, SOC is also in the low frequency domain because SOC change of 1% usually takes dozens of seconds even at a high power output/input. Therefore, both temperature and SOC are considered to be in the low frequency domain regarding their resolutions.

Table 1 describes the features of the multi-frequency recording method which cooperates two approaches according to the dynamic properties of signals. The flexible recording frequency approach is used in the low frequency domain for stationary signals, e.g. temperature, SOC, current and voltages during stationary charging. This approach records signals and the corresponding time when their values are changed regarding their resolutions. Fig. 1(A) demonstrates a typical signal which is suitable for the flexible recording frequency approach. The horizontal dotted lines indicate the signal resolution and the red dots are at the ideal recording time using the flexible recording frequency approach. The signal value changes slowly and not periodically with the time. Therefore, the "recording frequency" is flexible.

The recording frequency should be optimized for dynamic signals such as the current and voltages during dynamic charging/discharging. Fig. 1(B) demonstrates a typical signal which needs the approach of the recording frequency optimization. The vertical dotted lines indicate the recording period and the red[1] dots are uniformly distributed along the time axis according to the recording frequency. The most dynamic period can be observed in the figure. If the recording frequency is high enough to keep the signal undistorted in the most dynamic period, the whole signal will not be distorted. Procedures of the recording frequency optimization for dynamic signals are given in Fig. 1(C). Before the mass production of the BMS data logger, the demonstrated data logger will set to the maximum recording frequency f_{max} to record the dynamic signal for some time. During that time, the battery pack is required to operate in all working conditions so that the recorded signal will contain the most dynamic period. And then the signal is transformed using DWT which tells the most dynamic period during the whole operation. The most dynamic period of the signal is thereafter analyzed by FFT to find the essential frequencies contained in the signal which have higher amplitude. By determining the threshold of the essential frequencies, the optimal recording frequency is determined according to the sampling theorem. The data loggers under mass production will always use the optimized recording frequency for the signal as long as the working conditions of the battery pack are similar.

Battery data were collected in a developing BMS before the release of a demonstrated EV. The EV was tested in an automotive proving grounds for weeks. And for ten hours during the test, the EV covered all working conditions and the data logger was set to the maximum recording frequencies the system can provide for all signals: the recording frequency for temperatures and SOCs is approximately 1 Hz and the recording frequency for current and voltages is around 4 Hz (f_{max} = 4 Hz). We believe that if a recording frequency was found to be optimal under such a test, it would be redundant to other working conditions.

Temperature and SOC of Cell 1 as well as the total current and the mean voltage recorded during the test are displayed in Fig. 2. Because the test mainly contains an intensive dynamic discharging and followed by a constant charging, all signals exhibit two phases. Temperature in Fig. 2(A) raises from 15 °C to 22 °C in the first phase and maintains during the second phase. The insignificant change of the temperature during 10 h presents itself as a stationary signal. SOC in Fig. 2(B) is also stationary. It falls from 100% to 10% approximately during the intensive dynamic discharging and raises back to about 100% in the second phase.

The total current and the mean voltage in Fig. 2(C) are very dynamic during the first phase and become stationary during the constant charging. The total current and the mean voltage require the recording frequency optimization for the first phase and the flexible recording frequency approach in the second phase. Fortunately, the charging and idle state signals from BMS will tell

[1] For interpretation of color in Figs. 1, 3, 5, 6, 8, and 9, the reader is referred to the web version of this article.

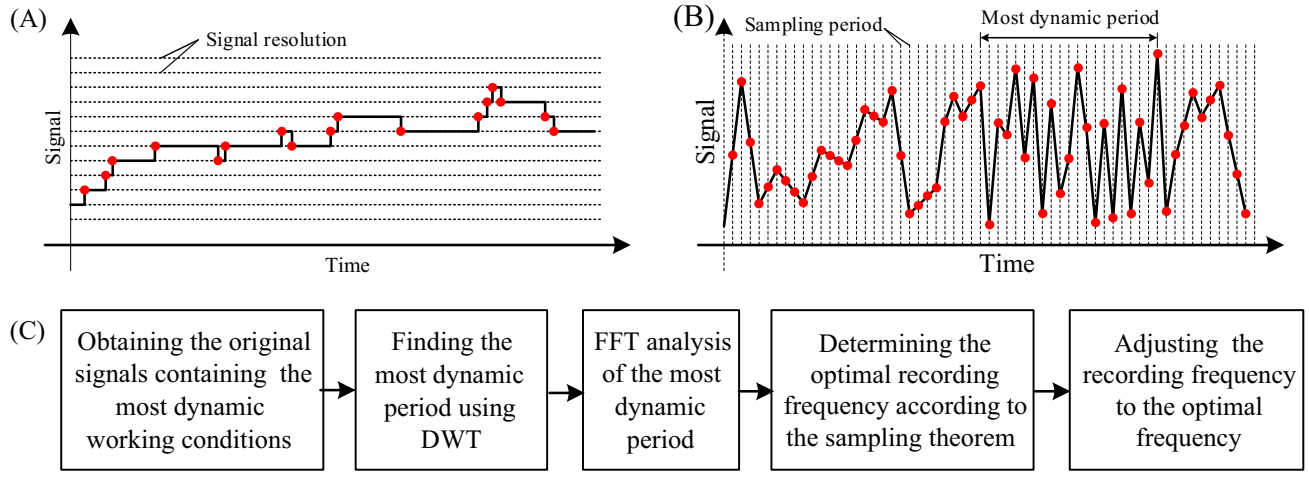

Fig. 1. Schematic diagram of the typical signals and signal recording frequency optimization procedures (A) typical signal can be recorded with flexible recording frequency approach (B) typical signal need to optimize the recording frequency and (C) recording frequency optimization procedures for dynamic signals.

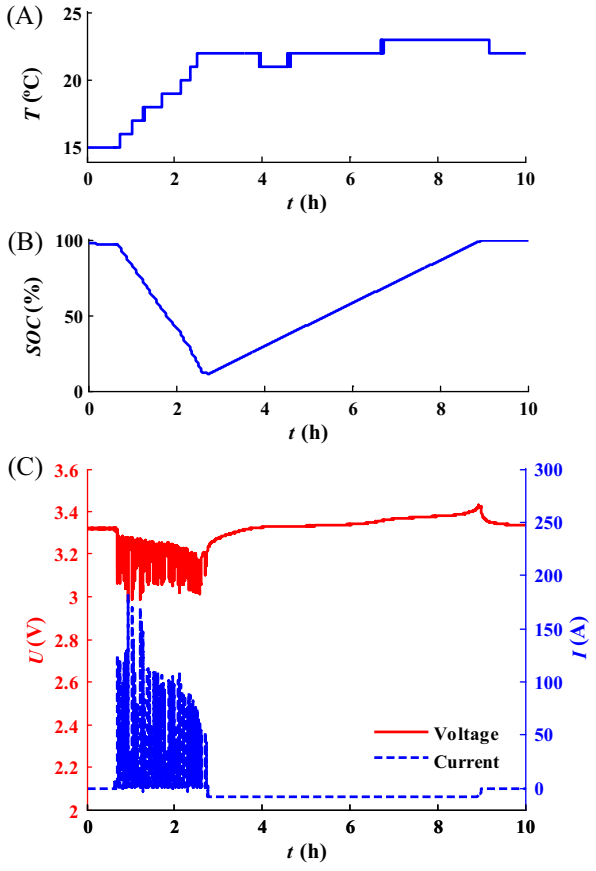

Fig. 2. Recorded signals with the maximum frequencies during the test (A) temperature of Cell 1 (B) SOC of Cell 1 and (C) mean voltage and total current.

the data logger to distinguish the two phases and makes the multi-frequency recording method feasible for online applications.

3. The flexible recording frequency approach for stationary signals

The temperatures, SOCs, voltages and the current in the second phase are recorded with the flexible recording frequency approach because they perform as stationary signals as shown in Fig. 2.

The flexible recording frequency approach for the temperature of Cell 1 are demonstrated for an instance. Fig. 3(A) gives the flowchart for recording the temperature immediately when the signal is changed and it is indicated as Method A. The basic idea is quite simple: the incoming value is compared to the latest recorded value and if the difference is less than the threshold θ, the incoming value and time will not be recorded. The threshold θ for temperature here is set to 1 °C which is the same as the recording accuracy. The result of Method A for the temperature recording is shown in Fig. 3(C) and its details from 6.7 h to 6.8 h are shown in Fig. 3(D) in the red circles. It is obvious that recording with Method A for the temperature not only keeps the signal undistorted but also has a significant reduction of the signal length.

The details of Method A in Fig. 3(D) suggests that some measurement disturbance occurs during the change of the temperature and it greatly increases the recording signal length using Method A in such cases. To further reduce the recording length, we proposed Method B which records the value after the signal is changed for p times. The flowchart of Method B is shown in Fig. 3(B). An obvious difference from Method A is that when the difference between the incoming value and the latest recorded value is larger than the threshold θ, the incoming value and time will not be recorded immediately. Instead, it will be first written to a buffer. When the difference between the incoming value and the latest recorded value is consecutively larger than the threshold θ for p times, the value in the buffer is then recorded.

The threshold θ for the temperature using Method B is also set to 1 °C which is the same as that in Method A. And p is 3 here, which means if the difference between the following 3 incoming values and the latest recorded value are always larger than the 1 °C, the first incoming value will be recorded. The result of Method B for the temperature recording is shown in Fig. 3(C) and its details from 6.7 h to 6.8 h are shown in Fig. 3(D) in the black crosses. Although the recorded signal with Method B shows a little difference from the original signal, it reduces the signal length a lot compared to that with Method A. Besides, the real temperature alteration point might be closer to the recorded signal with Method B rather than the original signal because of the measurement disturbance.

We quantitatively compare the recorded signals using different methods with the original signal as shown in Table 2. Three methods are compared here: Methods A and B, and the traditional fixed recording frequency method which records temperature value once every minute. According to the requirement of the signal

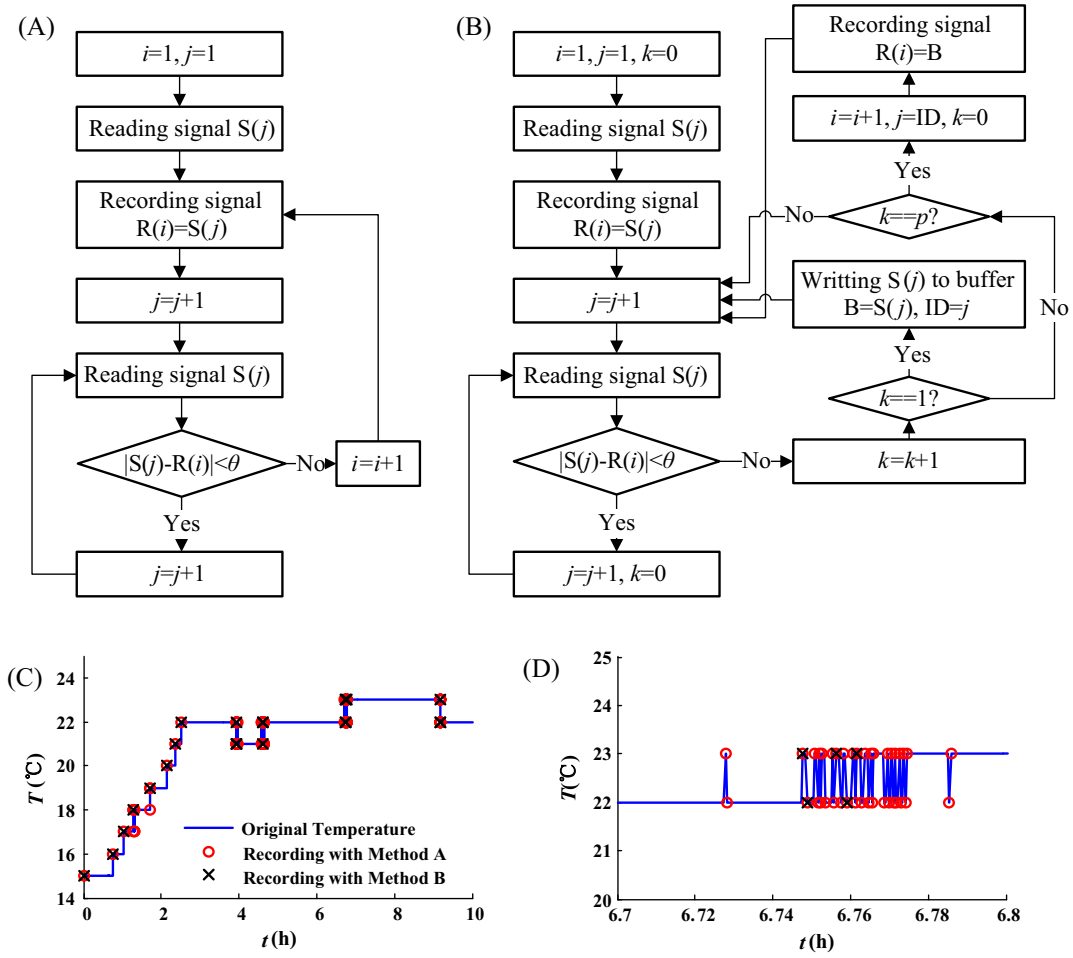

Fig. 3. Temperature recording using the flexible recording frequency approach (A) Method A: recording the signal immediately when the signal is changed (B) Method B: recording the signal after the signal is changed for p times (C) Comparison of the original temperature and recorded ones using the flexible recording frequency approach and (D) details of original and recorded temperatures from 6.7 h to 6.8 h.

Table 2
Comparing the recorded temperature signals using different methods with the original temperature signal.

	Signal length	Signal distortion (RMSE/°C)
Original signal	25,752	0
Fixed recording (1 min)	601	0.1092
Method A	142	0
Method B	22	0.0540

recording, two essential indicators are used: the signal length indicates the required storage memory and the signal distortion stands for the ability to keep the original signal. The signal distortion is calculated as the root mean square error (RMSE) between the recorded signal and the original signal. As seen in Table 2, the signal length of one-minute recording method is 601, and the signal distortion is 0.1092 °C. However, the signal length using Method B is only 22 with a decreasing signal distortion of 0.054 °C.

The SOC, the charging voltage and the charging current are similarly recorded using Method B with $p = 3$ as shown in Fig. 4. The indicators of the signals with the one-minute recording method and Method B are listed in Table 3. The signal length of the SOC recording with Method B is longer than that of one-minute recording method, because the threshold θ here is set to 0.1% SOC. As a result, the distortion is much smaller compared to the one-minute recording method. Regarding the charging voltage and current, thresholds here are 1 mV and 0.1 A respectively. The indicators of the recorded signals using Method B are all far better than that using one-minute recording method.

4. Recording frequency optimization for dynamic signals

4.1. Finding the most dynamic period

As we mentioned in Section 2, the recording frequency for the current and voltages during dynamic charging/discharging should be optimized. And we also explained that if the recording frequency is optimized for the current, we could use the same recording frequency for the voltages. Finally, Fig. 1(B) suggested that if the recording frequency is high enough to keep the signal undistorted in the most dynamic period, the whole signal will not be distorted. Hence, the very thing need to do for dynamic signals in data loggers is to optimize the recording frequency of the current during the most dynamic period.

Before we may implement the recording frequency optimization, the most dynamic period of the current in Fig. 2(C) during the first phase need to be examined. As no definition has been introduced to quantitatively measure the signal dynamic, one usually subjectively considers a signal to be dynamic according to his observation. As a result, it would be ambiguous to find the most dynamic period of the current. Nevertheless, the amplitude and frequency can always be used to describe the signal dynamic: a signal with a higher amplitude at a higher frequency is obviously more dynamic.

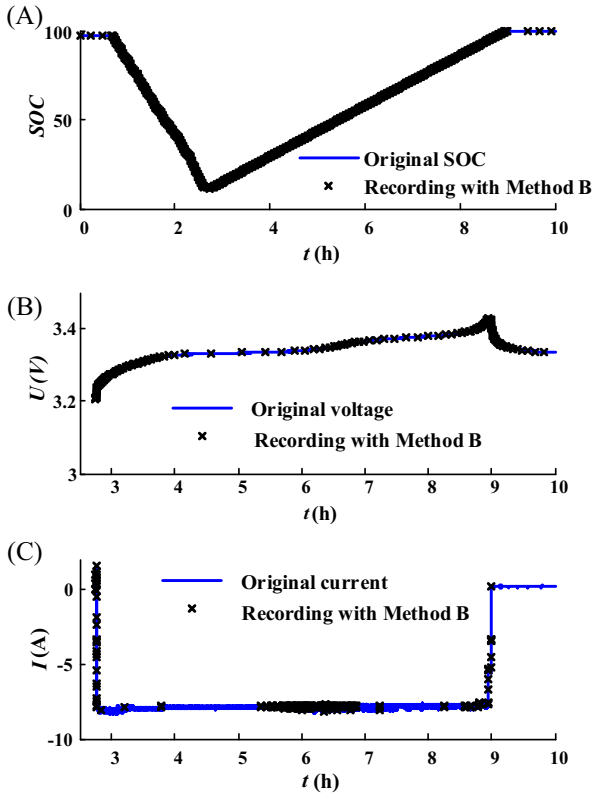

Fig. 4. The flexible recording frequency approach for (A) SOC (B) charging voltage and (C) charging current.

Fourier transformation looks a promising candidate to solve the issue mentioned above because the method is expert in the signal frequency analysis with the corresponding amplitudes. However, this method is unable to exhibit the information about time. As a result, the most dynamic period cannot be found with the Fourier transformation. Considering the information about time, short-time Fourier transform or DWT is a feasible choice. Here, we use DWT to examine the most dynamic period as DWT is one of the most powerful time-frequency-transformations because of the varied time-frequency window compared to the short-time Fourier transform. Kim et al. [27] presents a thorough application for a Li-ion cell based on the DWT. They suggested the order 3 Daubechies wavelet (dB3) as the mother wavelet, and the decomposition level was 5.

Hence, we use Matlab® wavelet toolbox to do the DWT using dB3 and 5 levels for our data in Fig. 2(C) during the first phase. The DWT absolute coefficients are displayed in Fig. 5(A), and the figure reads as follows: the horizontal axis indicates the time; the vertical axis represents the decomposition level, where the low levels represent high frequency component of the signal and the high levels represent the low frequency part; the values indicated by the pink color map can be considered as the signal amplitudes at the corresponding time and frequency. A larger amplitude at a lower level means the signal at that time can be expected to be more dynamic.

Because the most dynamic period should be a "period", we set the period $T_p = 60$ s. Thereafter, we calculate the mean signal amplitudes in the period T_p at Levels 1 and 2 every one second to determine the most dynamic period from the time interval 2313 s to 9471 s which covers the dynamic period in the first phase. Every mean signal amplitude from the time interval 2313 s to 9471 s at each level may be expressed as Eq. (2)

$$A_k(j) = \sum_{i=1}^{T_p \cdot f_{\max}} L_k(i/f_{\max} + j + 2312)/(T_p \cdot f_{\max}), \quad j = 1, 2, 3 \ldots 7100 \tag{2}$$

where $A_k(j)$ is the mean signal amplitude at time $j + 2312$ s, and $L_k(i/f_{\max} + j + 2312)$ is the absolute coefficient at time $i/f_{\max} + j + 2312$ s and Level k. As mentioned before, the data logger

Table 3
Comparing the fixed recording method and Method B with different signals.

		Original signal	Fixed recording (1 min)	Method B
SOC	Length	26,706	602	1559
	Distortion (RMSE/%)	0	0.2255	0.0569
Charging voltage	Length	104,295	435	169
	Distortion (RMSE/mV)	0	1.1	0.710
Charging current	Length	104,295	435	210
	Distortion (RMSE/A)	0	0.1542	0.0686

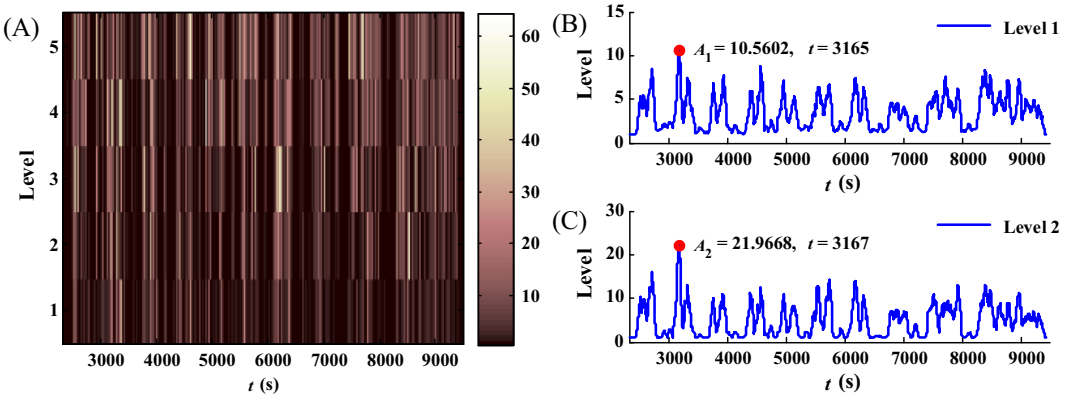

Fig. 5. (A) DWT absolute coefficients (B) mean signal amplitudes at Level 1 and (C) mean signal amplitudes at Level 2.

was set to the maximum recording frequency f_{max} = 4 Hz for the current.

The results are shown in Fig. 5(B) and (C). As marked by the red dots, the maximum values of the mean signal amplitudes locate at the time 3165 s and 3167 s respectively for Levels 1 and 2. It means the mean signal amplitude from 3165 s to 3225 s is the maximum at Level 1 and the mean signal amplitude from 3167 s to 3227 s is the maximum at Level 2. Because a larger mean signal amplitude at low levels can be expected to be a more dynamic period, we can say that the most dynamic period is around 3165 s to 3225 s.

From the engineering point of view, signal dynamics is usually measured using signal derivative. For the signal sequence of the current, the derivative can be calculated as Eq. (3)

$$dI(t) = (I(t+\Delta t) - I(t))/\Delta t = f_{max}(I(t+1/f_{max}) - I(t)) \quad (3)$$

The mean absolute derivative for every one second in the time window T_p is calculated,

$$\bar{dI}(j) = \sum_{i=1}^{T_p \cdot f_{max}} |dI(i/f_{max} + j + 2312)|/(T_p \cdot f_{max}), \quad j = 1, 2, 3 \ldots 7100 \quad (4)$$

where $\bar{dI}(j)$ is the mean absolute derivative at time j + 2312 s, and $dI(i/f_{max} + j + 2312)$ is the derivative at time $i/f_{max} + j + 2312$ s. The most dynamic period appears when $\bar{dI}(j)$ reaches the maximum value. The mean absolute derivative during the time interval 2313–9471 s is displayed in Fig. 6. As indicated by the red dot, the maximum value of the mean absolute derivative locates at the time 3165 s, which means the period 3165–3225 s can be considered as the most dynamic period.

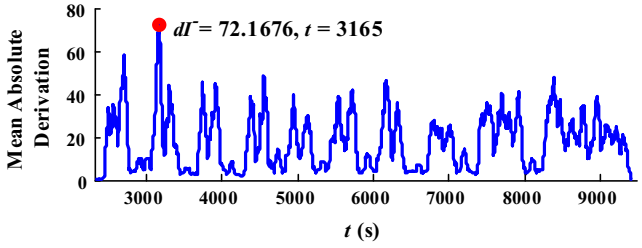

Fig. 6. The mean absolute derivation during the time interval 2313–9471 s.

As the result suggests, the most dynamic period from the mean absolute derivative method is the same as that from the DWT method. Besides, the correlation between $\bar{dI}$ and A_1 is 0.9788, so we may say $\bar{dI}$ and A_1 are similar. Because the mean absolute derivative method has less computation effort, it can be used for on-line determination of the most dynamic period for the current.

4.2. Recording frequency optimization

The most dynamic period of the current achieved in Section 4.1 is shown in Fig. 7(A). As the figure shows, the current swings swiftly between 0 and 125 A in this minute. To analyze the current frequency and amplitude, FFT is implemented. Because the direct current (DC) component of the current is not important, and also because FFT of the DC component has a large amplitude at zero frequency which will make the amplitudes of the other frequencies insignificant, we directly ignore the DC component in the following analysis. The signal length in the time domain is 241, so we set the signal length in the frequency domain to be 256. Doing so can speed up the computation of the FFT when the signal length in the time domain is not an exact power of 2. As the maximum recording frequency for the current is f_{max} = 4 Hz, the analyzed maximum FFT frequency is half of f_{max}. The FFT result is shown in Fig. 7(B). As the figure shows, the amplitude is set to 0 at f = 0 because the DC component is subtracted. The analyzed maximum FFT frequency is 2 Hz, and the plotted FFT frequency length is 128 which is a half of the signal length in the frequency domain.

The amplitude of the FFT signal generally declines with the frequency, which manifests that the current mainly consists of low frequency components. Besides, the amplitude is significantly small when the signal frequency is larger than 1.2 Hz, which indicates the maximum recording frequency f_{max} = 4 Hz is ample for the current recording.

Four characterized frequencies are investigated to determine which frequency is suitable for the current storage. As demonstrated in Fig. 7(B), the four characterized frequencies are f_1 = 0.5 Hz, f_2 = 0.68 Hz, f_3 = 1 Hz, and f_4 = 1.2 Hz respectively. According to the sampling theorem, the recording frequencies are f_{s1} = 1 Hz, f_{s2} = 1.36 Hz, f_{s3} = 2 Hz, and f_{s4} = 2.4 Hz correspondingly.

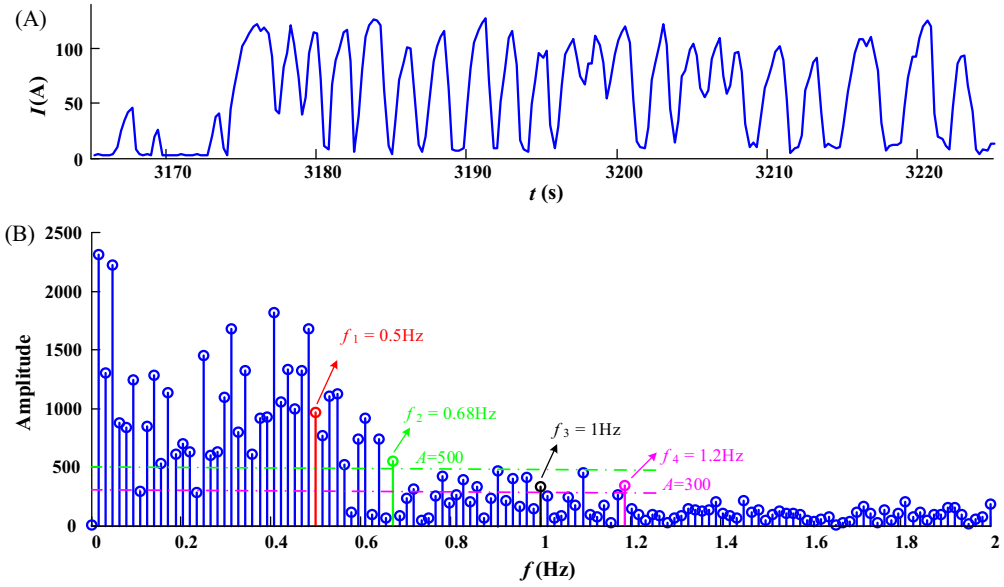

Fig. 7. (A) The most dynamic period of the current from 3165 to 3225 s and (B) FFT analysis of the most dynamic period of the current.

Because the recording frequencies f_{s1} = 1 Hz and f_{s3} = 2 Hz are the common engineering choices, the corresponding characterized frequencies f_1 = 0.5 Hz and f_3 = 1 Hz are naturally to be investigated. Regarding the characterized frequencies f_2 = 0.68 Hz and f_4 = 1.2 Hz, they are determined when the amplitudes are always less than the thresholds (500 and 300 in Fig. 7(B) respectively) with the further increasing frequencies.

Data storage at the above recording frequencies implies that higher frequency signal components are not considered any more. For example, the recording frequency f_{s1} = 1 Hz will discard signal components with the frequencies higher than f_1 = 0.5 Hz. Obviously, for the recording frequency f_{s1} = 1 Hz, a lot of the signal components are discarded, because the signal with the frequencies higher than f_1 = 0.5 Hz still have considerable amplitudes. Therefore, we may expect that large signal distortion is inevitable with the recording frequency f_{s1} = 1 Hz in this case.

Comparison between the current signals with four recording frequencies and the original current with the maximum recording frequency f_{max} = 4 Hz is shown in Fig. 8. The current with solid blue curve in Fig. 8 is recorded at 4 Hz and is considered as the original signal. The current with the dashed red curve in Fig. 8(A) is recorded at 1 Hz. As we expected, signal distortion is clearly observed especially during the time intervals 3176–3184 s, 3197–3202 s and 3205–3208 s. By increasing the recording frequency to 1.36 Hz, as shown in the dashed green curve in Fig. 8

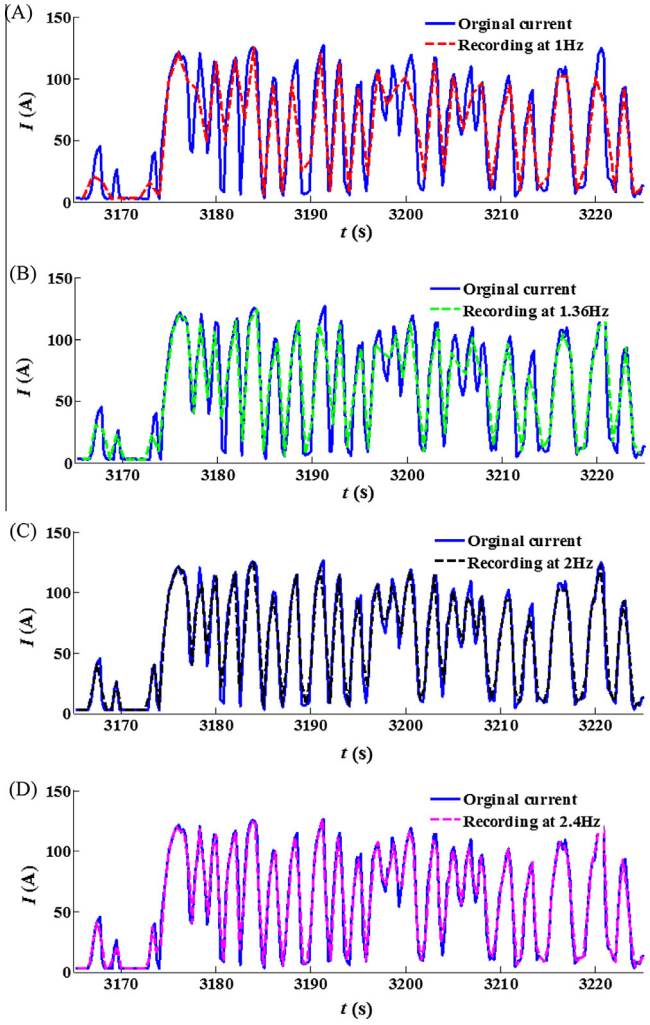

Fig. 8. Comparison between the current signals with four recording frequencies and the original current. Recording at (A) 1 Hz (B) 1.36 Hz (C) 2 Hz and (D) 2.4 Hz.

Table 4
Comparison the current and mean voltage with four recording frequencies with the original signals.

	Signal length	Current distortion (RMSE/A)	Mean voltage distortion (RMSE/mV)
Original signal (4Hz)	28,701	0	0
Recording at 1 Hz	7183	7.85	11.5
Recording at 1.36 Hz	9768	5.90	8.6
Recording at 2 Hz	14,365	4.02	5.8
Recording at 2.4 Hz	17,238	3.39	4.8

(B), the distortion decreases a lot because the amplitudes of the signal components from f_1 to f_2 are considerable. However, with the recording frequency of 1.36 Hz, signal distortion is still obvious during the time interval 3197–3202 s and 3205–3208 s.

By increasing the recording frequency to 2 Hz, as shown in the dashed black curve in Fig. 8(C), signal distortion is no longer significant. However, as shown in the dashed magenta curve in Fig. 8(D), further increasing the recording frequency to 2.4 Hz seems no help to improve the signal quality as the amplitudes of the signal components from f_3 to f_4 are relatively small.

We again use the signal length to indicate the required storage memory and RMSE to measure the signal distortion. To examine the overall dynamic current signal, we use the dynamic current in Fig. 2(C) during the first phase instead of the most dynamic period we found. The indicator results are shown in Table 4. The signal length recorded at 1 Hz is the least, but the current distortion is the most with RMSE of 7.85A. By increasing the recording frequency, the signal length increases, but the current distortion decreases.

4.3. Discussion

It is difficult to tell whether the current distortion with an RMSE of 7.85 A or 3.39 A is qualified for the current recording. Hence, we further investigate the mean voltage distortion in Table 4. The measurement accuracy for the cell voltage is commonly demanded at 5 mV in engineering and 1 mV in experiments [28,29]. As a result, we can see that recording at 1 Hz is not qualified even we set the accuracy to 10 mV for the cell voltage recording. Recording at 1.36 Hz is acceptable when the recording accuracy is not important. And if we want the accuracy of the recorded cell voltage to be as high as the measurement accuracy in engineering, we need to increase the recording frequency to at least 2 Hz in the working condition of the development EV.

To further examine the reliability of the data at the recording frequency of 2 Hz compared to the original signals which were recorded at 4 Hz, we use the SOC estimation which is one of the most concerned issues in BMS to evaluate the data. Three typical SOC estimation methods are commonly used for on-line application: the OCV method, the ampere hour method and EKF based estimations [30]. The OCV method requires the battery to be rested for some time (several hours especially when the battery is at low temperatures [31]). Therefore, the flexible recording frequency approach for stationary signals is used. The measured voltage by this method is almost the same as the original voltage, because we set the threshold for the voltage to be 1 mV in this method. Hence, it will not reduce the accuracy of the SOC estimation by the OCV method.

Regarding SOC estimation using the ampere hour method, currents recording at 2 Hz and 4 Hz (the original current) are compared. Because the ampere hour method uses the current integration, the only thing we need to do is to show the difference between the current integration values using different recording frequencies. The current integration values (Ah) and the difference between the two recording frequencies from the time interval

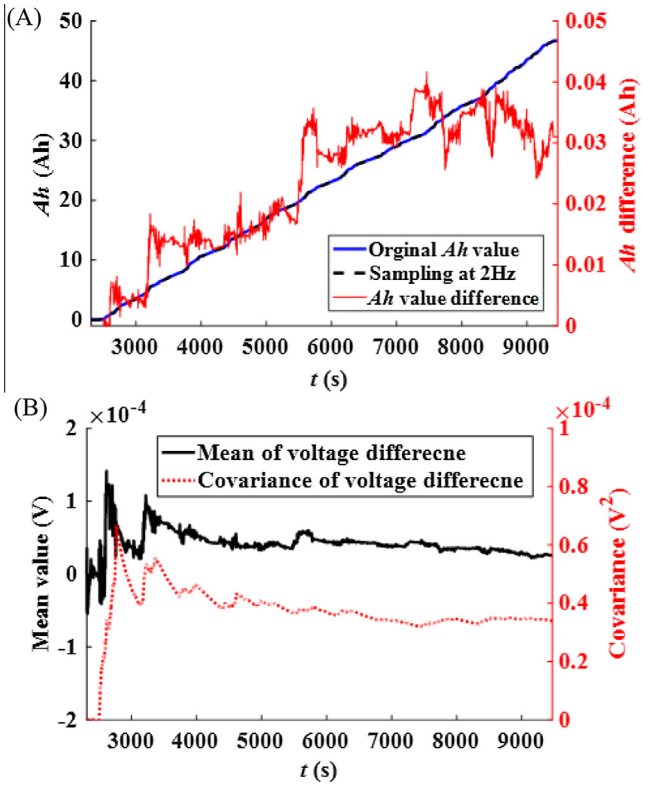

Fig. 9. Influences on SOC estimation when signals are recorded at the optimal recording frequency compared to the original signals. (A) Current influence using ampere hour method and (B) voltage influence using EKF based estimation method.

2313 s to 9471 s are shown in Fig. 9(A). The blue curve shows the current integration value with the original current, and the black dashed curve which represents the current integration value at 2 Hz is almost the same as the blue curve. The difference is also plotted in the red curve where the maximum difference is about 0.04 Ah only accounting for 0.1% of the total current integration value. Therefore, current recording at 2 Hz will not influence the SOC estimation using the ampere hour method compared to the original current.

The well-known EKF based SOC estimation has its general discrete-time equations as

$$\begin{aligned} \boldsymbol{x}_{k+1} &= \boldsymbol{A}\boldsymbol{x}_{k+1} + \boldsymbol{B}\boldsymbol{x}_{k+1} + \omega_k \\ \boldsymbol{y}_{k+1} &= \boldsymbol{C}\boldsymbol{x}_{k+1} + \boldsymbol{D}\boldsymbol{x}_{k+1} + \upsilon_k \end{aligned} \tag{5}$$

$\boldsymbol{y}_{k+1}$ is usually the voltage output and υ_k is the measurement (or observation) noise which is assumed to be Gaussian white noise with zero mean and covariance $\boldsymbol{R}_k$ [32]. Therefore, the voltage is needed to be observed in the EKF based SOC estimation. When the recording frequency is reduced from 4 Hz to 2 Hz, the voltage difference between the two recording frequencies from the time interval 2313 s to 9471 s exhibits itself as a white noise with the mean and covariance plotted in Fig. 9(B). The absolute value of the mean voltage difference is less than 0.2 mV and the covariance is far less than 0.0001 V^2. This means the voltage difference can be treated as a part of the measurement noise υ_k. As a consequence, it will have a negative influence on the convergence behavior but the accuracy of the SOC estimation would not be influenced.

From the above analysis, we may see that though using the optimal recording frequency may remove some "information" from the original signals, the removed "information" is however mostly white noise with no information. As a result, the accuracy of the SOC estimation is not influenced.

5. Conclusion

Massive data storage in BMS can provide statistical and individual working conditions of battery packs which support the further development of EVs. The optimal recording frequency in practice should be as low as possible on the condition that little signal distortion happens. In this paper, we present a novel method which uses a multi-frequency recording technology according to the signal dynamics.

Firstly, dynamic properties of signals in BMS are discussed. Temperature, SOC, the current and voltages during stationary charging are low frequency signals. While the current and voltages during dynamic charging and discharging are high frequency signals. The multi-frequency recording technology according to the signal dynamics is then proposed.

For low frequency signals, a flexible recording frequency method is applied which only records signals when their values are changed. Compared to the fixed recording frequency, the recorded signal length is drastically shortened with the additional benefit of even lower signal distortion.

For dynamic signals, the most dynamic period is successfully found using DWT. The mean absolute derivative method also verifies the most dynamic period from the engineering point of view. The most dynamic period is further analyzed by FFT. By comparing two recording signal indicators for four different recording frequencies, we conclude that recording at 1 Hz is not qualified during the dynamic period in our system due to the high dynamic performance of the vehicle. Only by increasing the recording frequency to at least 2 Hz, can the accuracy of the recorded cell voltage achieve the level the same as the measurement accuracy in engineering.

With the flexible recording frequency approach proposed in this paper, the signal length is shortened and the signal distortion is lowered for low frequency signal in BMS. For the dynamic current and voltage recording, with the procedures proposed in this paper, the optimal recording frequency can be suggested according to the working conditions which helps the determination of the recording frequency during the BMS development. And by comparing the signals with different recording frequencies, we also concluded that when the recording frequency is reduced to the optimal frequency compared the high frequency recorded original signals, the accuracy of the SOC estimation is not influenced. This will provide a solid support for on-line SOC estimation when different recording frequencies are used.

Acknowledgment

This research is supported by the National Natural Science Foundation of China (NSFC) under the Grant number of 51507102, the State Key Laboratory of Automotive Safety and Energy under Project No. KF16022, and the Science and Technology Foundation of State Grid Corporation of China (SGCC) under the contract number of DG71-14-032. The data were provided by Beijing Keypower Tech. Co.

References

[1] Li X, Hui D, Lai X. Battery energy storage station (BESS)-based smoothing control of photovoltaic (PV) and wind power generation fluctuations. IEEE Trans Sustain Energy 2013;4:464–73.
[2] Schuster SF, Brand MJ, Berg P, Gleissenberger M, Jossen A. Lithium-ion cell-to-cell variation during battery electric vehicle operation. J Power Sources 2015;297:242–51.
[3] Kenney B, Darcovich K, MacNeil DD, Davidson IJ. Modelling the impact of variations in electrode manufacturing on lithium-ion battery modules. J Power Sources 2012;213:391–401.
[4] Gogoana R, Pinson MB, Bazant MZ, Sarma SE. Internal resistance matching for parallel-connected lithium-ion cells and impacts on battery pack cycle life. J Power Sources 2014;252:8–13.

[5] Truchot C, Dubarry M, Liaw BY. State-of-charge estimation and uncertainty for lithium-ion battery strings. Appl Energy 2014;119:218–27.
[6] Klee Barillas J, Li J, Günther C, Danzer MA. A comparative study and validation of state estimation algorithms for Li-ion batteries in battery management systems. Appl Energy 2015;155:455–62.
[7] Zhang K, Xu L, Ouyang M, Wang H, Lu L, Li J, et al. Optimal decentralized valley-filling charging strategy for electric vehicles. Energy Convers Manage 2014;78:537–50.
[8] Amoroso FA, Cappuccino G. Impact of charging efficiency variations on the effectiveness of variable-rate-based charging strategies for electric vehicles. J Power Sources 2011;196:9574–8.
[9] Zheng Y, Lu L, Han X, Li J, Ouyang M. $LiFePO_4$ battery pack capacity estimation for electric vehicles based on charging cell voltage curve transformation. J Power Sources 2013;226:33–41.
[10] Zheng Y, Ouyang M, Lu L, Li J, Han X, Xu L. On-line equalization for lithium-ion battery packs based on charging cell voltages: Part 1. Equalization based on remaining charging capacity estimation. J Power Sources 2014;247:676–86.
[11] Waag W, Fleischer C, Sauer DU. Critical review of the methods for monitoring of lithium-ion batteries in electric and hybrid vehicles. J Power Sources 2014;258:321–39.
[12] Xiong R, Sun F, Chen Z, He H. A data-driven multi-scale extended Kalman filtering based parameter and state estimation approach of lithium-ion polymer battery in electric vehicles. Appl Energy 2014;113:463–76.
[13] Mahamud R, Park C. Reciprocating air flow for Li-ion battery thermal management to improve temperature uniformity. J Power Sources 2011;196:5685–96.
[14] Li X, Li J, Xu L, Ouyang M, Han X, Lu L, et al. Online management of lithium-ion battery based on time-triggered controller area network for fuel-cell hybrid vehicle applications. J Power Sources 2010;195:3338–43.
[15] Hauser A, Kuhn R. 11 – high-voltage battery management systems (BMS) for electric vehicles A2 – Scrosati, Bruno. In: Garche J, Tillmetz W, editors. Advances in battery technologies for electric vehicles. Woodhead Publishing; 2015. p. 265–82.
[16] Wang Y, Zhang C, Chen Z, Xie J, Zhang X. A novel active equalization method for lithium-ion batteries in electric vehicles. Appl Energy 2015;145:36–42.
[17] Gallardo-Lozano J, Romero-Cadaval E, Milanes-Montero MI, Guerrero-Martinez MA. A novel active battery equalization control with on-line unhealthy cell detection and cell change decision. J Power Sources 2015;299:356–70.
[18] Zheng Y, Han X, Lu L, Li J, Ouyang M. Lithium ion battery pack power fade fault identification based on Shannon entropy in electric vehicles. J Power Sources 2013;223:136–46.
[19] Feng X, Weng C, Ouyang M, Sun J. Online internal short circuit detection for a large format lithium ion battery. Appl Energy 2016;161:168–80.
[20] Hu C, Jain G, Zhang P, Schmidt C, Gomadam P, Gorka T. Data-driven method based on particle swarm optimization and k-nearest neighbor regression for estimating capacity of lithium-ion battery. Appl Energy 2014;129:49–55.
[21] Li Y, Chattopadhyay P, Ray A. Dynamic data-driven identification of battery state-of-charge via symbolic analysis of input–output pairs. Appl Energy 2015;155:778–90.
[22] Zheng Y, Ouyang M, Lu L, Li J. Understanding aging mechanisms in lithium-ion battery packs: from cell capacity loss to pack capacity evolution. J Power Sources 2015;278:287–95.
[23] ALL NIPPON AIRWAYS CO., LTD. Aircraft Serious Incident Investigation Report. Japan Transport Safety Board; 2014, AI2014-4.
[24] Offer GJ, Yufit V, Howey DA, Wu B, Brandon NP. Module design and fault diagnosis in electric vehicle batteries. J Power Sources 2012;206:383–92.
[25] You G, Park S, Oh D. Real-time state-of-health estimation for electric vehicle batteries: a data-driven approach. Appl Energy 2016;176:92–103.
[26] Khayyam H, Abawajy J, Javadi B, Goscinski A, Stojcevski A, Bab-Hadiashar A. Intelligent battery energy management and control for vehicle-to-grid via cloud computing network. Appl Energy 2013;111:971–81.
[27] Kim J, Cho BH. An innovative approach for characteristic analysis and state-of-health diagnosis for a Li-ion cell based on the discrete wavelet transform. J Power Sources 2014;260:115–30.
[28] Zheng Y, Ouyang M, Lu L, Li J, Han X, Xu L, et al. Cell state-of-charge inconsistency estimation for $LiFePO_4$ battery pack in hybrid electric vehicles using mean-difference model. Appl Energy 2013;111:571–80.
[29] Lu L, Han X, Li J, Hua J, Ouyang M. A review on the key issues for lithium-ion battery management in electric vehicles. J Power Sources 2013;226:272–88.
[30] Perez G, Garmendia M, Francois Reynaud J, Crego J, Viscarret U. Enhanced closed loop State of Charge estimator for lithium-ion batteries based on Extended Kalman Filter. Appl Energy 2015;155:834–45.
[31] Waag W, Sauer DU. Adaptive estimation of the electromotive force of the lithium-ion battery after current interruption for an accurate state-of-charge and capacity determination. Appl Energy 2013;111:416–27.
[32] Sun F, Xiong R, He H. A systematic state-of-charge estimation framework for multi-cell battery pack in electric vehicles using bias correction technique. Appl Energy 2016;162:1399–409.